

Supporting Information

[α -AsW₉O₃₃]⁹⁻ bridged hexagonal cluster of Ln (III) showing field induced SMM behavior: an experimental and theoretical insight

Sandhya Kapurwan, Pradip Kumar Sahu, Mukul Raizada, Ranjan Kharel, Sanjit Konar*^a

^a Department of Chemistry, Indian Institute of Science Education and Research (IISER), Bhopal By-pass Road, Bhauri, Bhopal-462066, India

Table S1. Crystal data and structure refinement for Complexes **1-4**.

Sample Code	Complex 1 (Er-POM)	Complex 2 (Gd-POM)
Empirical formula	As ₆ Cs ₁₂ Er ₆ K ₂₄ O ₂₅₂ W ₅₄	As ₆ Cs ₈ Gd ₆ K ₂₈ O ₂₄₆ W ₅₄
Formula weight	17946.30	17415.00
Temperature/K	100.0	100.00
Crystal system	triclinic	triclinic
Space group	P-1	P-1
a/ \AA	19.550(4)	19.484(5)
b/ \AA	19.813(4)	19.619(5)
c/ \AA	22.294(5)	19.740(4)
$\alpha/^\circ$	113.140(8)	109.682(9)
$\beta/^\circ$	96.931(8)	93.416(9)
$\gamma/^\circ$	110.158(7)	92.743(10)
Volume/ \AA^3	7119(3)	7074(3)
Z	1	1
$\rho_{\text{calc}}/\text{cm}^3$	4.186	4.088
μ/mm^{-1}	26.115	25.457
F(000)	7734.0	7518.0
Crystal size/mm ³	0.1 \times 0.08 \times 0.05	0.1 \times 0.08 \times 0.05
Radiation	MoK α ($\lambda = 0.71073$)	MoK α ($\lambda = 0.71073$)
2 Θ range for data collection/ $^\circ$	3.55 to 50.182	4.004 to 50.282
Index ranges	-23 \leq h \leq 23, -23 \leq k \leq 23, -26 \leq l \leq 26	-23 \leq h \leq 23, -23 \leq k \leq 23, -23 \leq l \leq 23
Reflections collected	233322	279602
Independent reflections	25161 [Rint = 0.1191, Rsigma = 0.0623]	25063 [Rint = 0.1169, Rsigma = 0.0562]
Data/restraints/parameters	25161/6/967	25063/0/966
Goodness-of-fit on F ²	1.037	1.077
Final R indexes [$I >= 2\sigma(I)$]	R1 = 0.0514, wR2 = 0.1355	R1 = 0.0531, wR2 = 0.1461
Final R indexes [all data]	R1 = 0.0603, wR2 = 0.1433	R1 = 0.0695, wR2 = 0.1516
Largest diff. peak/hole / e \AA^{-3}	5.60/-6.46	5.18/-7.63

Sample Code	Complex 3 (Ho-POM)	Complex 4 (Tb-POM)
Empirical formula	As ₆ Cs ₁₂ Ho ₆ K ₂₄ O ₂₃₈ W ₅₄	As ₆ Cs ₁₅ K ₂₁ O ₂₁₆ Tb ₆ W ₅₄
Formula weight	17708.32	17601.69
Temperature/K	100.00	120.0
Crystal system	triclinic	trigonal
Space group	P-1	P-3
a/ \AA	18.891(3)	23.461(2)
b/ \AA	19.724(3)	23.461(2)
c/ \AA	21.788(4)	14.730(2)
$\alpha/^\circ$	68.133(6)	90
$\beta/^\circ$	87.425(7)	90
$\gamma/^\circ$	64.508(6)	120
Volume/ \AA^3	6736(2)	7021.8(16)
Z	1	1
$\rho_{\text{calc}}/\text{g/cm}^3$	4.365	4.163
μ/mm^{-1}	27.485	26.516
F(000)	7616.0	7536.0
Crystal size/mm ³	0.1 × 0.08 × 0.05	0.1 × 0.08 × 0.05
Radiation	MoK α ($\lambda = 0.71073$)	MoK α ($\lambda = 0.71073$)
2 Θ range for data collection/ $^\circ$	4.434 to 52.954	3.472 to 48.902
Index ranges	-23 ≤ h ≤ 23, -24 ≤ k ≤ 24, -27 ≤ l ≤ 27	-27 ≤ h ≤ 27, -27 ≤ k ≤ 27, -17 ≤ l ≤ 17
Reflections collected	275842	85910
Independent reflections	27687 [Rint = 0.1222, Rsigma = 0.0620]	7736 [Rint = 0.1570, Rsigma = 0.0739]
Data/restraints/parameters	27687/0/922	7736/0/300
Goodness-of-fit on F ²	1.103	1.091
Final R indexes [I>=2σ (I)]	R1 = 0.0638, wR2 = 0.1502	R1 = 0.0849, wR2 = 0.1993
Final R indexes [all data]	R1 = 0.0995, wR2 = 0.1745	R1 = 0.1501, wR2 = 0.2624
Largest diff. peak/hole / e \AA^{-3}	5.68/-7.48	6.77/-4.20

Table S2. Selected bond distances (\AA) for complexes **1-4**.

Er1-O1	2.308(12)	Gd1-O29	2.462(16)	Ho1-O16	2.275(17)
Er1-O28	2.266(12)	Gd1-O30	2.305(18)	Ho1-O20	2.344(17)
Er1-O34	2.376(12)	Gd1-O31	2.426(17)	Ho1-O34	2.362(17)
Er1-O37	2.437(12)	Gd1-O32	2.440(17)	Ho1-O35	2.442(17)
Er1-O38	2.347(13)	Gd1-O94	2.290(16)	Ho1-O76	2.354(18)
Er1-O39	2.329(12)	Gd1-O98	2.441(16)	Ho1-O77	2.417(18)
Er1-O67	2.381(13)	Gd1-O99	2.434(18)	Ho1-O82	2.376(18)
Er1-O68	2.374(13)	Gd1-O106	2.368(17)	Ho1-O93	2.412(17)
Er2-O45	2.302(12)	Gd2-O13	2.457(13)	Ho2-O18	2.373(16)
Er2-O46	2.300(13)	Gd2-O14	2.407(13)	Ho2-O19	2.425(17)
Er2-O69	2.341(15)	Gd2-O18	2.363(13)	Ho2-O24	2.409(18)
Er2-O70	2.344(14)	Gd2-O19	2.424(12)	Ho2-O28	2.364(17)
Er2-O71	2.352(11)	Gd2-O38	2.418(13)	Ho2-O36	2.277(17)
Er2-O72	2.420(12)	Gd2-O39	2.319(12)	Ho2-O39	2.318(17)
Er2-O73	2.340(13)	Gd2-O41	2.350(13)	Ho2-O69	2.360(2)
Er2-O74	2.393(12)	Gd2-O77	2.419(14)	Ho2-O70	2.360(2)
Er3-O4	2.354(11)	Gd3-O63	2.380(13)	Ho3-O44	2.371(17)
Er3-O5	2.418(11)	Gd3-O64	2.453(13)	Ho3-O45	2.428(17)
Er3-O13	2.320(12)	Gd3-O66	2.408(13)	Ho3-O50	2.417(17)
Er3-O20	2.405(12)	Gd3-O67	2.448(12)	Ho3-O57	2.370(17)
Er3-O100	2.267(12)	Gd3-O73	2.434(14)	Ho3-O71	2.300(17)
Er3-O101	2.379(12)	Gd3-O74	2.424(14)	Ho3-O72	2.258(16)
Er3-O102	2.370(12)	Gd3-O75	2.309(13)	Ho3-O73	2.410(2)
Er3-O103	2.282(12)	Gd3-O76	2.336(13)	Ho3-O74	2.404(19)

Tb(1)O(14)	2.38(3)	Tb(1)O(3)	2.36(3)
Tb(1)O(18)	2.39(3)	Tb(1)O(20)	2.42(3)
Tb(1)O(10)	2.37(3)	Tb(1)O(19)	2.45(3)
Tb(1)O(4)	2.41(3)	Tb(1)O(15)	2.35(2)

Table S3. Lanthanides geometry analysis by using Continuous Shape Measurements (CShM)²

[ML ₈]	OP-8	HPY-8	HBPY-8	CU-8	SAPR-8	TDD-8	JGBF-8	JETBP-Y-8	JBTP-R-8	BTPR-8	JSD-8	TT-8
Er1	33.699	23.247	14.929	9.830	2.082	2.278	14.314	29.498	2.155	1.435	4.799	10.448
Er2	33.656	23.473	14.667	9.116	2.163	1.776	14.663	29.067	2.185	1.418	4.485	9.731
Er3	34.185	23.417	15.130	9.256	1.917	1.856	14.989	29.353	2.163	1.444	4.675	9.920

[ML8]	OP-8	HPY-8	HBPY-8	CU-8	SAPR-8	TDD-8	JGBF-8	JETBP-Y-8	JBTPR-8	BTPR-8	JSD-8	TT-8
Gd1	34.184	23.394	15.307	9.768	2.035	2.164	15.178	29.821	2.322	1.481	4.953	10.432
Gd2	33.864	23.116	15.222	9.652	2.180	2.273	14.888	29.864	2.260	1.384	4.957	10.206
Gd3	33.821	23.283	14.715	9.307	2.211	2.118	14.566	28.973	2.205	1.441	4.873	9.888

[ML8]	OP-8	HPY-8	HBPY-8	CU-8	SAPR-8	TDD-8	JGBF-8	JETBP-Y-8	JBTPR-8	BTPR-8	JSD-8	TT-8
Ho1	34.414	23.096	15.494	9.770	1.920	1.975	14.861	29.650	2.162	1.355	4.708	10.443
Ho2	33.630	22.576	15.807	9.708	1.969	1.842	15.386	29.581	2.201	1.429	4.649	10.457
Ho3	34.073	23.477	15.526	10.108	2.013	2.329	14.558	29.515	2.217	1.388	4.743	10.848

[ML8]	OP-8	HPY-8	HBPY-8	CU-8	SAPR-8	TDD-8	JGBF-8	JETBP-Y-8	JBTPR-8	BTPR-8	JSD-8	TT-8
Tb1	33.929	23.271	15.106	9.626	1.918	2.162	14.685	29.629	2.255	1.238	4.870	10.419

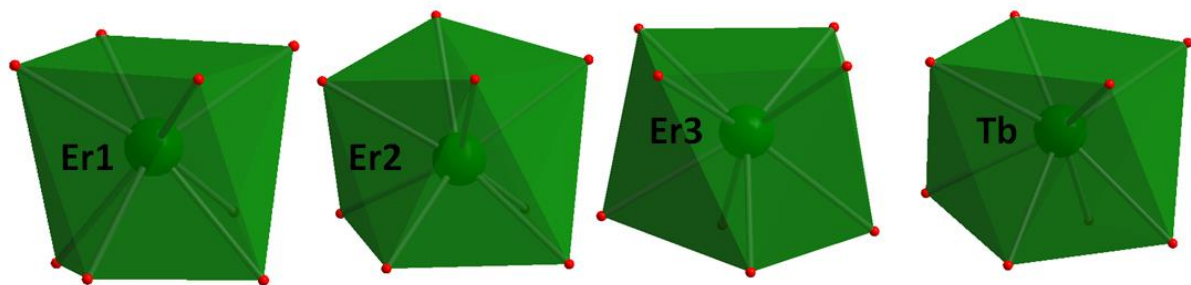


Fig S1. Polyhedral representation of binding sites of the metal centers for complexes **1&4**.

OP-8	D_{8h}	Octagon
HPY-8	C_{7v}	Heptagonal pyramid
HBPY-8	D_{6h}	Hexagonal bipyramid
CU-8	O_h	Cube
SAPR-8	D_{4d}	Square antiprism
TDD-8	D_{2d}	Triangular dodecahedron
JGBF-8	D_{2d}	Johnson gyrobifastigium J26
JETBPY-8	D_{3h}	Johnson elongated triangular bipyramid J14
JBTPR-8	C_{2v}	Biaugmented trigonal prism J50
BTPR-8	C_{2v}	Biaugmented trigonal prism
JSD-8	D_{2d}	Snub diphenoïd J84
TT-8	T_d	Triakis tetrahedron
ETBPY-8	D_{3h}	Elongated trigonal bipyramid

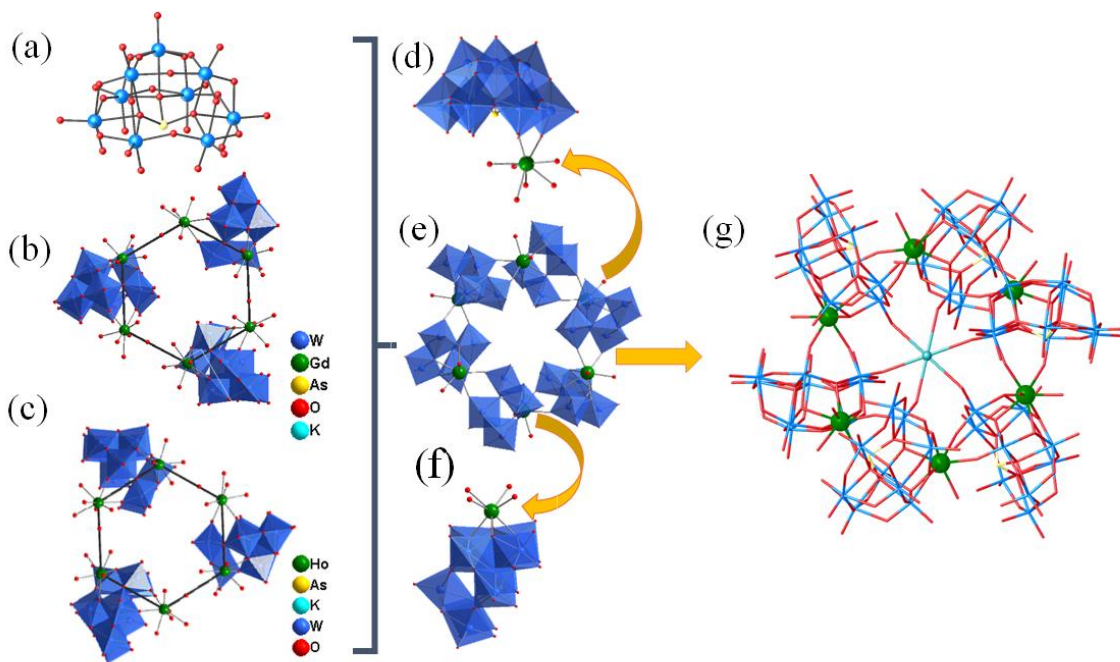


Fig. S2 (a) Ball and-stick representation of $[\alpha\text{-AsW}_9\text{O}_{33}]^{9-}$; (b) &(c) asymmetric unit representations, shows three different Gd and Ho centres in the asymmetric unit of complexes **2** and **3** and; (d) & (f) binding mode of Gd & Ho centres; (e) Polyhedral representation of simplest unit of complexes **2&3**; (f) Ball and stick representation of the cluster in complexes **2** & **3**. H atoms are omitted for clarity. Color code: WO₆ blue octahedra; Gd &Ho green; K cyan; O red.

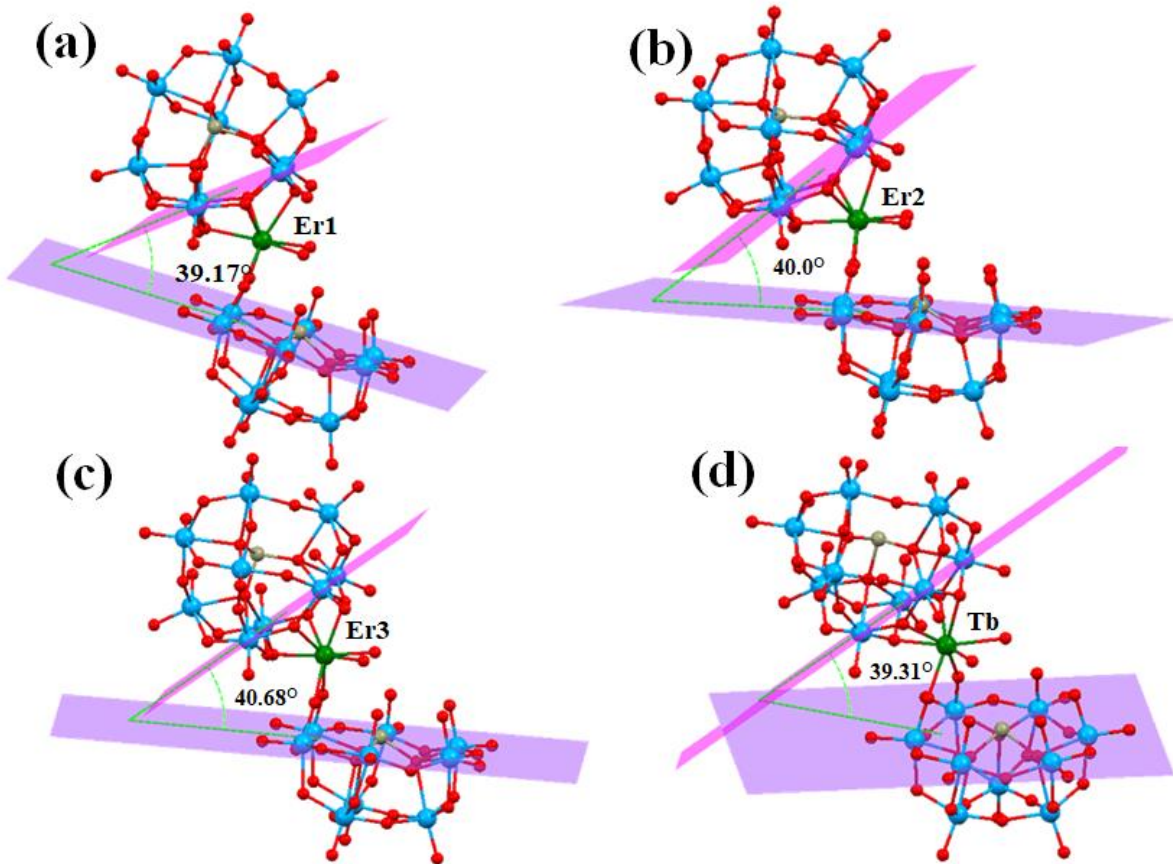


Fig. S3 Angle between the plane passes through W centers which directly coordinate with Ln centres (a) Er1 (b) Er2 (c) Er3 of complex **1** and (d) Tb of complex **4**. (Pink color represent the plane which passes thought the W centres bonded to terminal O atom coordinate to Ln centers and purple to the W of μ_2 -O coordinate to Ln centers).

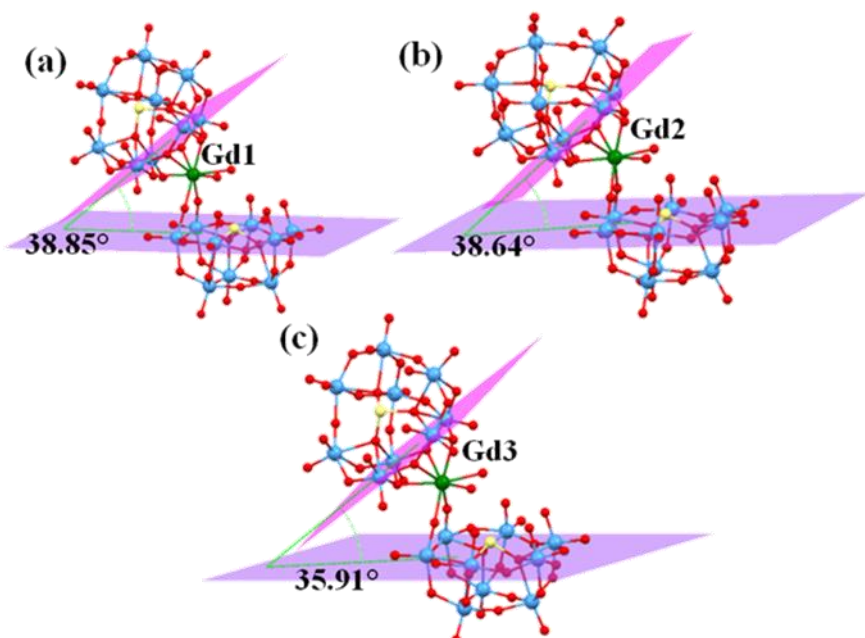


Fig. S4 Angle between the plane passes through W centers which directly coordinate with Ln centres (a) Gd1 (b) Gd2 and (c) Gd3 of complex **2**. (Pink color represent the plane which passes thought the W centres bonded to terminal O atom coordinate to Ln centers and purple to the W of μ_2 -O coordinate to Ln centers).

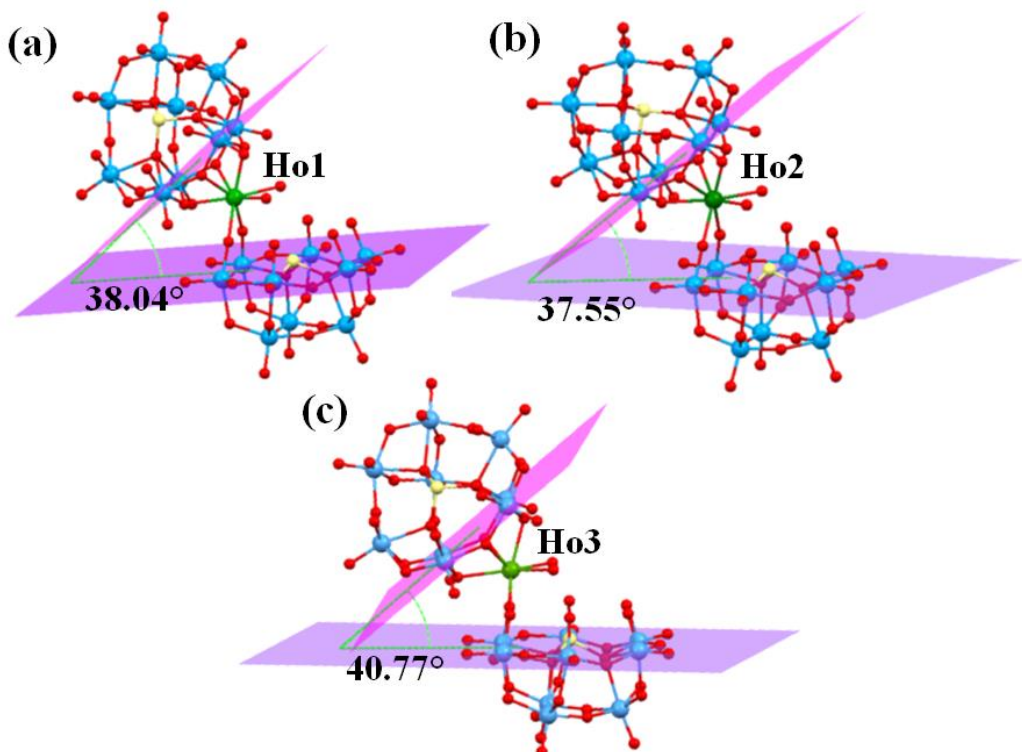


Fig. S5 Angle between the plane passes through W centers which directly coordinate with Ln centres (a) Ho1 (b) Ho2 and (c) Ho3 of complex **3**. (Pink colour represent the plane which passes thought the W centres bonded to terminal O atom coordinate to Ln centers and purple to the W of μ_2 -O coordinate to Ln centers).

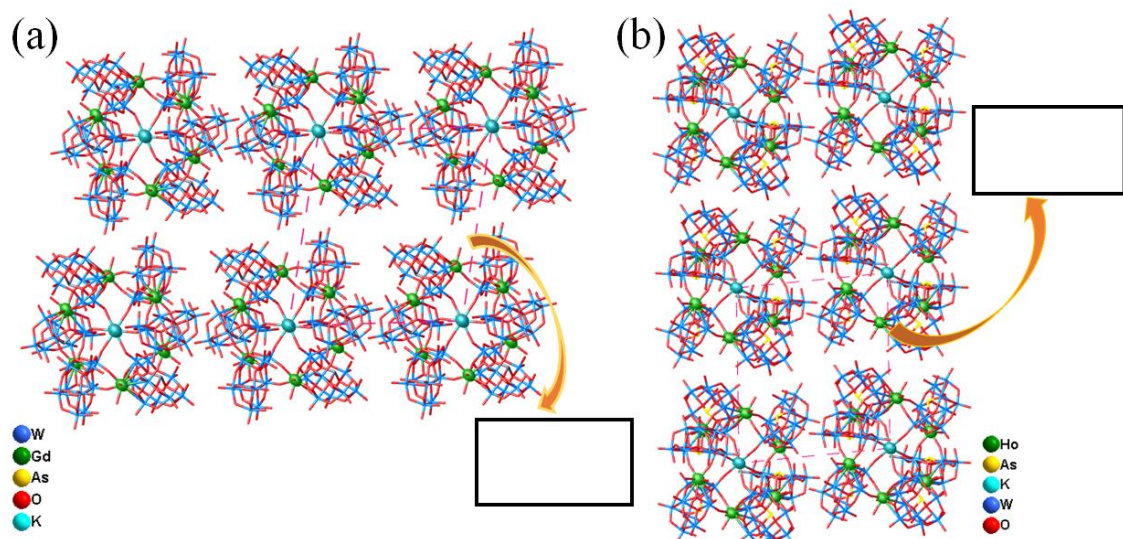


Fig. S6 Packing Diagram Complex **2** (a) & Complex **3** (b) along crystallographic *a* axis. Colors codes of Elements: Green = Gd & Ho. Pale yellow= As, Blue=W, Red= O and cyan= K.

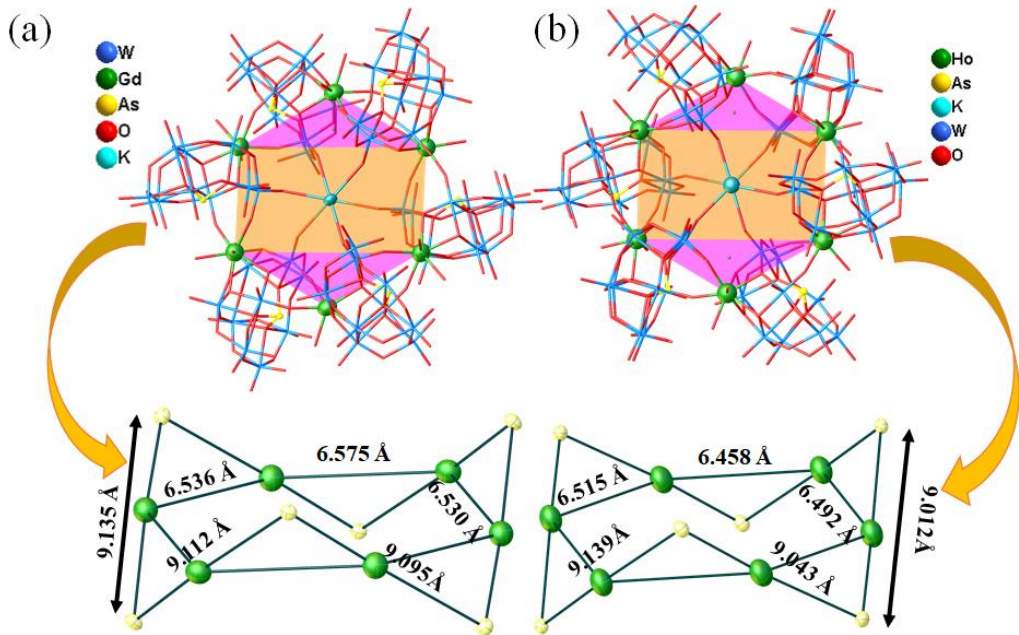


Fig. S7 The distorted cyclohexane-like framework in Complexes **2** (a) and **3** (b) formed by the connection of the six As(III) heteroatoms of the Heteropolyoxometalates units. Color code: As, pale yellow; Gd & Ho, green.

2. Additional measurements

Infrared Spectroscopy

The IR spectrum of **1-4** shows the skeletal vibrations in the region between 500 and 1200 cm⁻¹. A characteristic peak for the polyanion at 942 cm⁻¹ can be attributed to the terminal W–O_t vibrations. Broad peaks at 877 and 784 cm⁻¹ can be assigned to the two types of W–O–W stretching vibrations and the peak at 702 cm⁻¹ belongs to the W–O(–As) stretch. Additionally, broad peaks at 3350 cm⁻¹ and 1617 cm⁻¹ are mainly associated with the stretching and bending modes of lattice and coordinated water molecules.

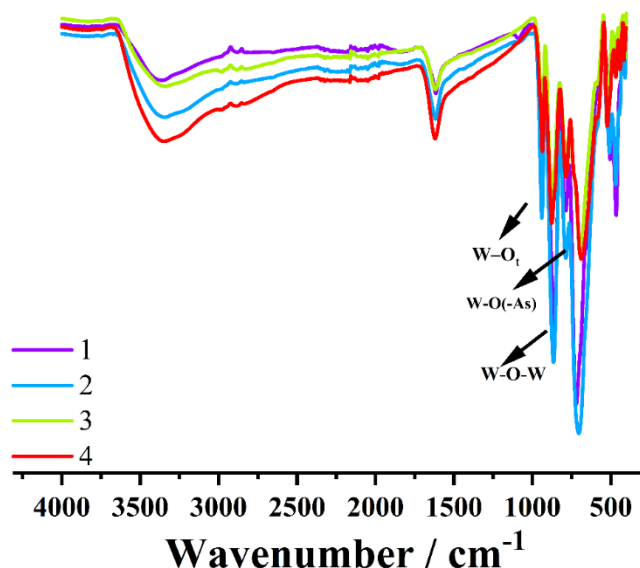


Fig. S8 Infrared spectrum for Complexes **1-4**.

Thermogravimetric analysis

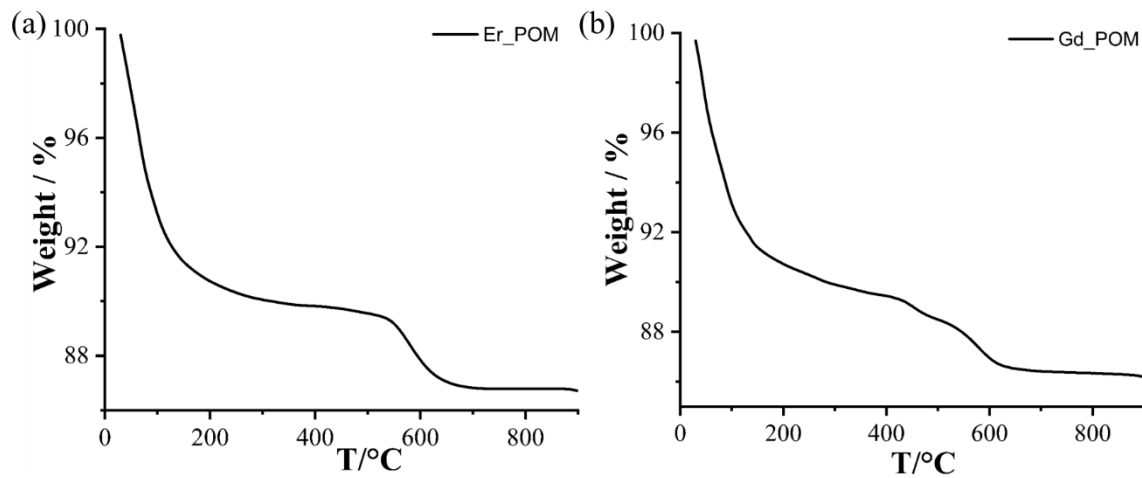


Fig. S9 Thermogravimetric (TG) curve of Complexes **1** (a) & **2** (b) under N_2 atmosphere (5 K min^{-1}).

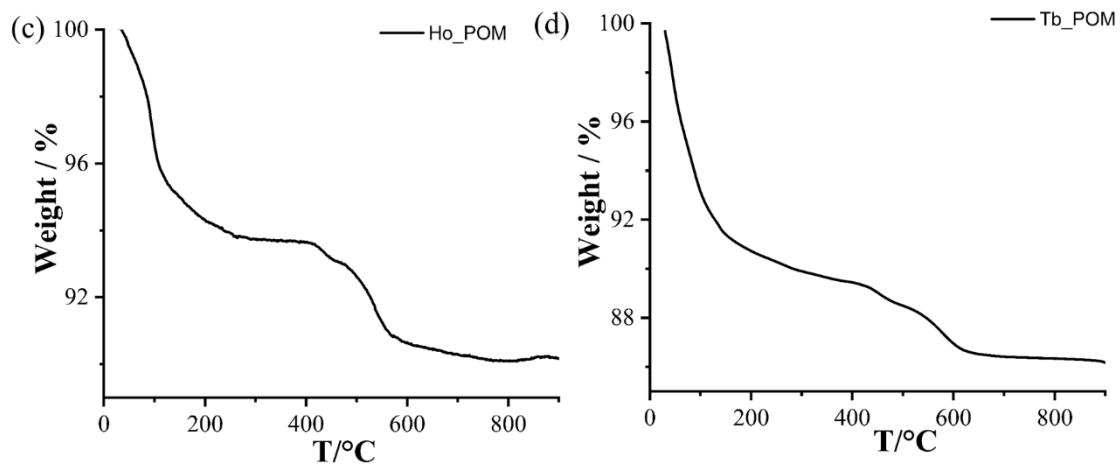


Fig. S10 Thermogravimetric (TG) curve of Complexes **3** (a) & **4** (b) under N_2 atmosphere (5 K min^{-1}).

3. PXRD Characterization

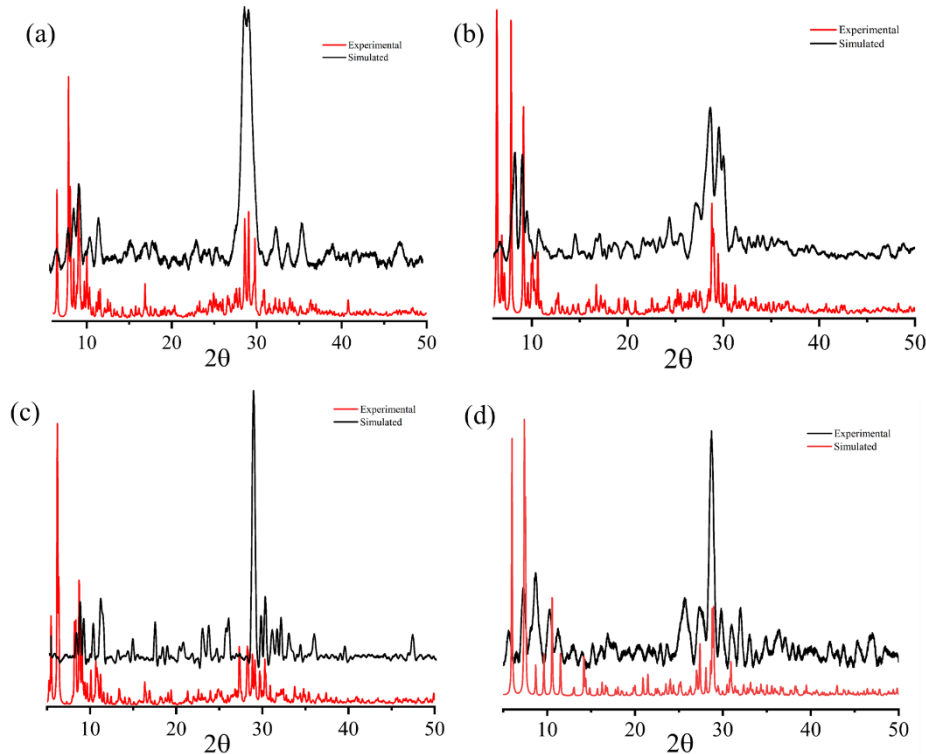


Fig. S11 Experimental and simulated PXRD pattern of complexes **1-4**.

3. EDX Characterization

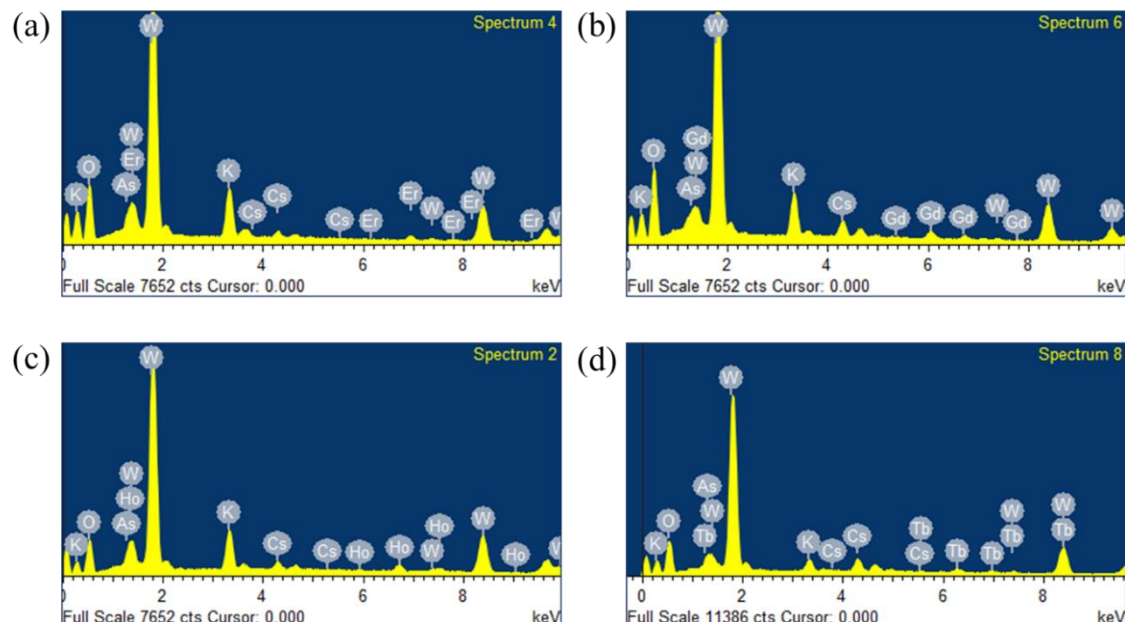


Fig. S12 EDX Data of complexes **1-4**.

3. Magnetic Characterization

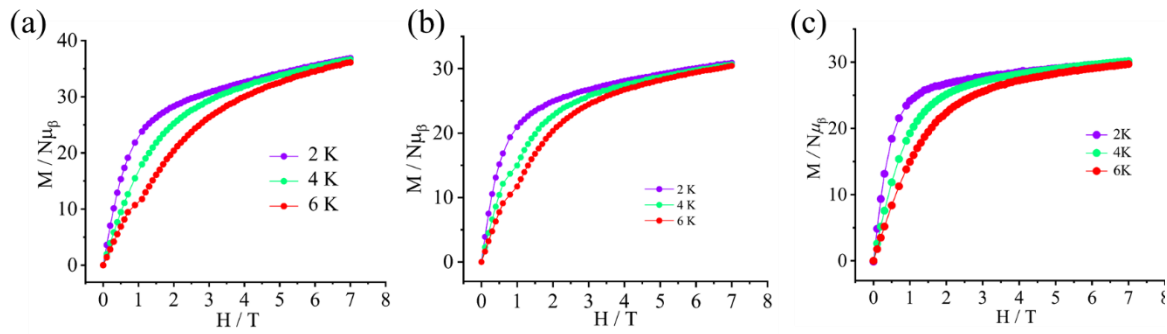


Fig. S13 Field dependent isothermal magnetization plot of complexes **1**, **3**, and **4** at 2, 4, 6 K.

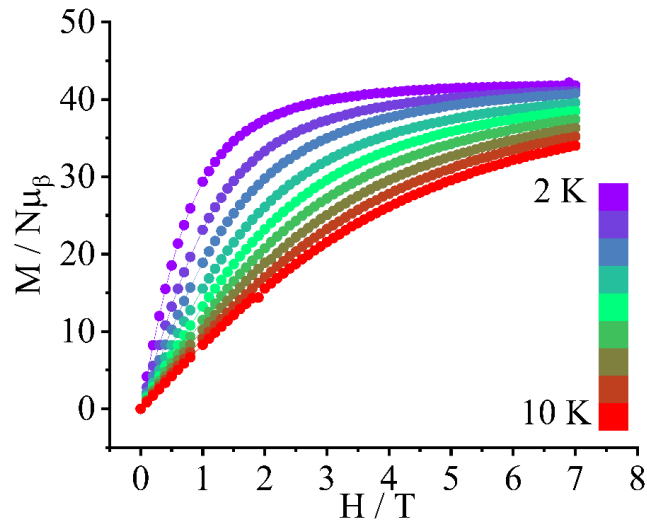


Fig. S14 Field dependent isothermal magnetization plot of complex **2**.

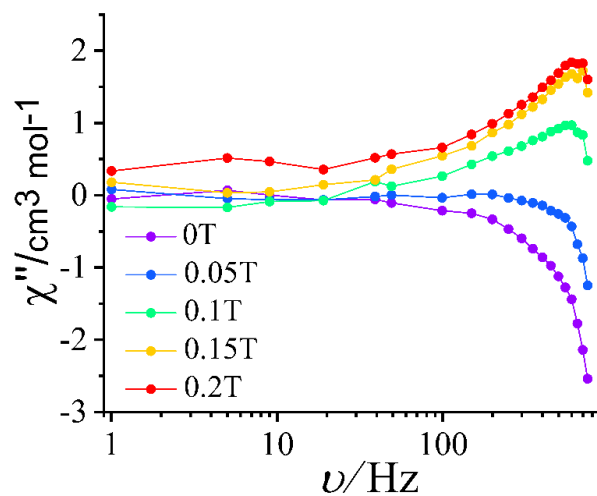


Fig. S15 The out-of-phase ac susceptibility under different external magnetic field for complex **1**.

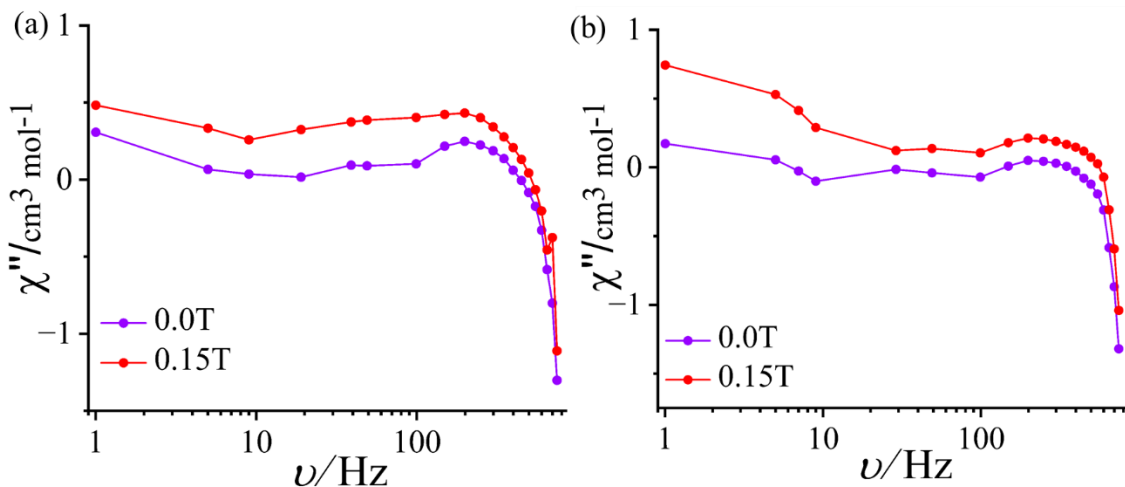


Fig. S16 The frequency dependent out-of-phase ac susceptibility plot of complex **3** (a) and **4** (b) with different magnetic field.

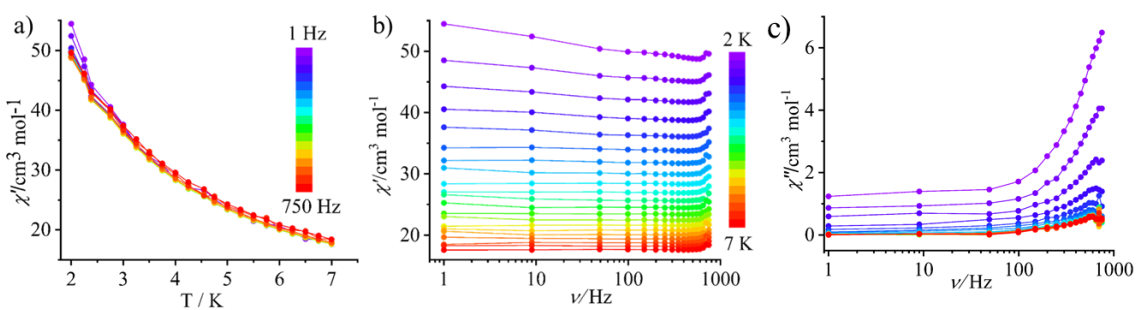


Fig. S17 Temperature (a) and frequency (b & c) dependent in-phase and out-of-phase ac susceptibility under 1500 Oe external magnetic field for complex **1**.

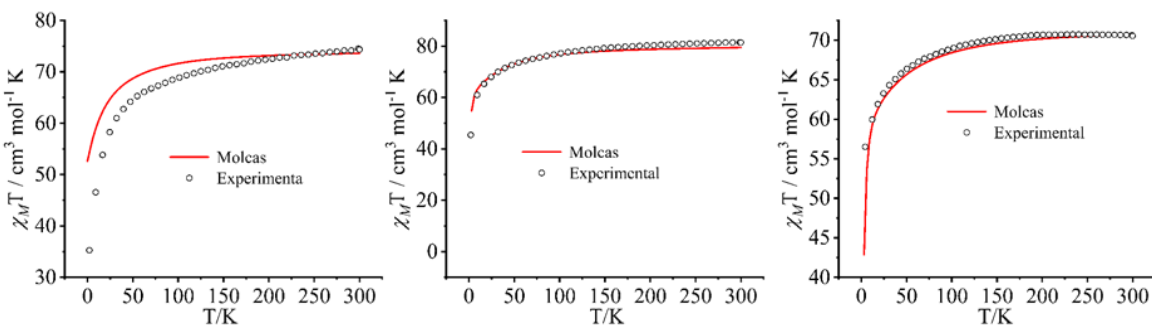


Fig. S18 Experimental and *ab initio* calculated magnetic susceptibility plot for complexes **1**, **3** and **4**

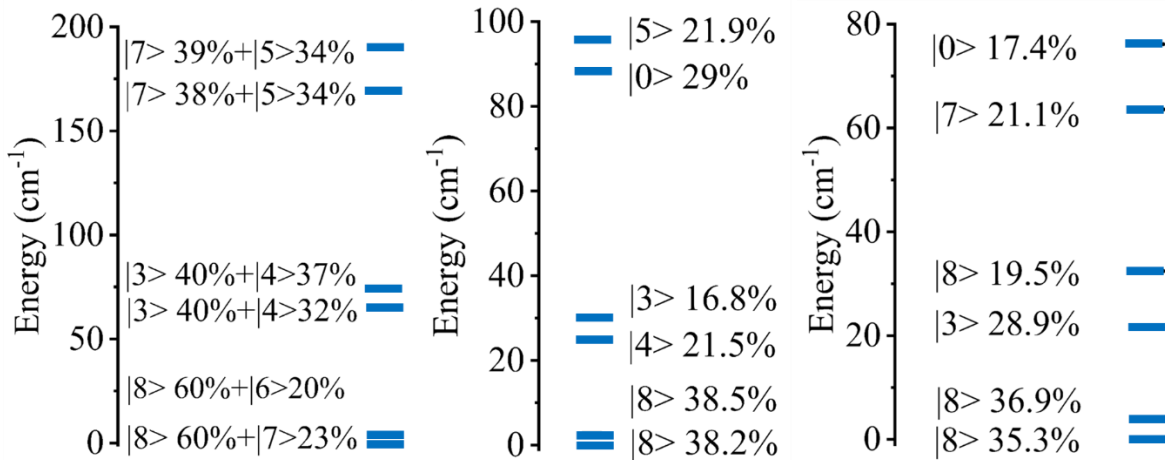


Fig. S19 CF split energy levels calculated by *ab initio* for Ho (III) centre in complex **3**.

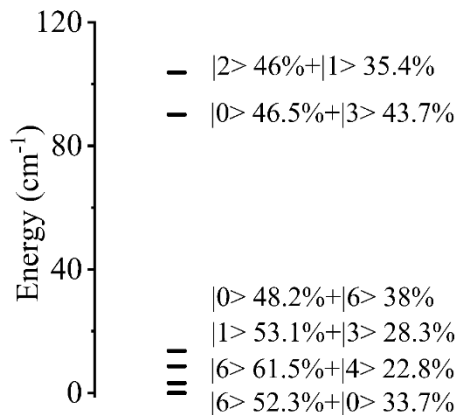


Fig. S20 CF split energy levels calculated by *ab initio* for Tb(III) centre in complex **4**.

Table S4: CASSCF+RASSI-SO+SINGLE_ANISO calculated energy spectrum, values of the g tensors of the pseudo-doublets, and wavefunctions compositions of each state for complex **1**

Kramers doublets	Er1			Er2			Er3		
GS	0 cm ⁻¹	gx = 0.15 gy = 0.74 gz = 16.80	88.7% ±15/2>	0 cm ⁻¹	gx = 1.46 gy = 4.68 gz = 12.75	54.7% ±15/2> + 15.7% ±11/2>	0 cm ⁻¹	gx = 0.47 gy = 2.40 gz = 14.95	39% ±15/2>
st 1 ES	57.6 cm ⁻¹	gx = 2.35 gy = 3.60 gz = 12.02	59.9% ±13/2> + 25.8% ±9/2>	13.4 cm ⁻¹	gx = 2.44 gy = 2.77 gz = 12.84	18.2% ±9/2> + 16% ±5/2>	31.1 cm ⁻¹	gx = 0.83 gy = 2.05 gz = 14.12	39% ±9/2> + 14.7% ±5/2>
nd 2 ES	102.9 cm ⁻¹	gx = 7.91 gy = 6.14 gz = 2.37	41% ±13/2> + 31% ±5/2>	55.7 cm ⁻¹	gx = 1.28 gy = 3.96 gz = 8.77	15.1% ±15/2>	74.7 cm ⁻¹	gx = 0.31 gy = 3.27 gz = 10.25	20% ±1/2> + 16.6% ±11/2>

Table S5: SINGLE_ANISO computed crystal-field parameters for complex **1**

k, q	B_q^k (Er1)	B_q^k (Er2)	B_q^k (Er3)
2, -2	+1.9	-15.3	-0.18
2, -1	-1.9	+0.52	-0.14
2, 0	-1.57	-5.78	-4.27
2, 1	-0.98	-2.62	-2.03
2, 2	+1.28	-7.64	+0.16
4, -4	-0.02	+0.14	+0.028
4, -3	-0.11	+0.091	+0.047
4, -2	+0.003	+0.019	+0.01
4, -1	-0.066	-0.01	+0.027
4, 0	-0.001	-0.015	+0.362
4, 1	-0.018	+0.037	+0.006
4, 2	-0.017	+0.009	-0.02
4, 3	+0.001	-0.059	+0.037
4, 4	-0.044	-0.25	-0.032

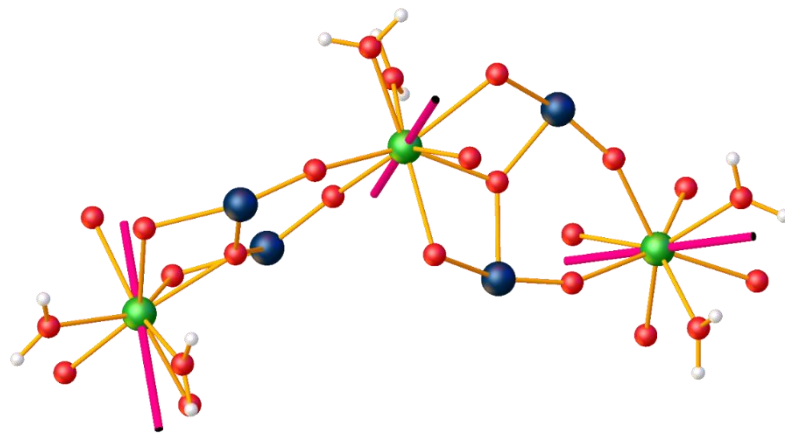


Fig. S21 Orientation of anisotropic axes (pink line) in the computed fragment of complex **1**. Color code: green-Er, blue-W, red O, white H.

Table S6: CASSCF+RASSI-SO+SINGLE_ANISO calculated energy spectrum, values of the g tensors of the pseudo-doublets, and wave function compositions of each state for complex **3**

Ising/ Pseudo doublets	Ho1			Ho2			Ho3		
1 2	0 cm ⁻¹ 0.1 cm ⁻¹	g _x = 0 g _y = 0 g _z = 18.57	60% ±8>+23 % ±7>	0 cm ⁻¹ 2.6 cm ⁻¹	g _x = 0 g _y = 0 g _z = 17.84	38.5% ±8>	0 cm ⁻¹ 4.1 cm ⁻¹	g _x = 0 g _y = 0 g _z = 17.15	35.3% ±8>
3 4	42.25 cm ⁻¹ 42.85 cm ⁻¹	g _x = 0 g _y = 0 g _z = 19.13	40% ±3>+32 % ±4>	24.9 cm ⁻¹ 30 cm ⁻¹	g _x = 0 g _y = 0 g _z = 16.10	21.5% ±4> and 16.8% ±3>	21.6 cm ⁻¹ 32.4 cm ⁻¹	g _x = 0 g _y = 0 g _z = 14.88	28.9% ±3> and 19.65 % ±3>
5 6	92.01 cm ⁻¹ 93.55 cm ⁻¹	g _x = 0 g _y = 0 g _z = 16.12	38% ±7>+4 % ±5>	88.4 cm ⁻¹ 95.7 cm ⁻¹	g _x = 0 g _y = 0 g _z = 12.27	21.9% ±5> and 29% ±0>	63.5 cm ⁻¹ 76.1 cm ⁻¹	g _x = 0 g _y = 0 g _z = 8.78	21.1% ±7> and 17.4 % ±4>

Table S7: SINGLE_ANISO computed crystal-field parameters for complex **3**

k, q	B_q^k (Ho1)	B_q^k (Ho2)	B_q^k (Ho3)
2, -2	-0.50	-8.75	-3.34
2, -1	+0.54	+6.67	-11.06
2, 0	-1.40	-6.13	-4.52
2, 1	+2.88	-5.7	-2.03
2, 2	-2.75	+11.2	+5.55
4, -4	+0.021	-0.15	-0.053
4, -3	+0.093	+0.17	-0.176
4, -2	+0.016	-0.022	-0.007
4, -1	-0.005	-0.026	-0.025
4, 0	-0.001	+0.008	+0.001
4, 1	-0.011	+0.037	-0.003
4, 2	+0.034	+0.013	-0.087
4, 3	+0.133	+0.113	-0.111
4, 4	+0.016	+0.062	-0.097

Table S8: CASSCF+RASSI-SO+SINGLE_ANISO calculated energy spectrum, values of the g tensors of the pseudo-doublets, and wavefunctions compositions of each state for complex **4**

Ising/Pseudo doublets	Tb		
1	0 cm ⁻¹	gx = 0	61.5% ±6>+22.8 % ±4>
2	3.1 cm ⁻¹	gy = 0 gz = 13.93	
3	8.6 cm ⁻¹	gx = 0	28.3% ±3>+53.1 % ±1>
4	13.5 cm ⁻¹	gy = 0 gz = 13.17	
5	90.1 cm ⁻¹	gx = 0	43.7% ±3>+46.5 % ±0>
6	103.7 cm ⁻¹	gy = 0 gz = 13.4	

Table S9: SINGLE_ANISO computed crystal-field parameters for complex **4**

k, q	B_q^k (Tb)
2, -2	+0.18
2, -1	+0.36
2, 0	-0.70
2, 1	-1.92
2, 2	+5.00
4, -4	+0.004
4, -3	+0.011
4, -2	+0.003
4, -1	+0.004
4, 0	-0.001
4, 1	+0.011
4, 2	+0.020
4, 3	-0.048
4, 4	+0.018

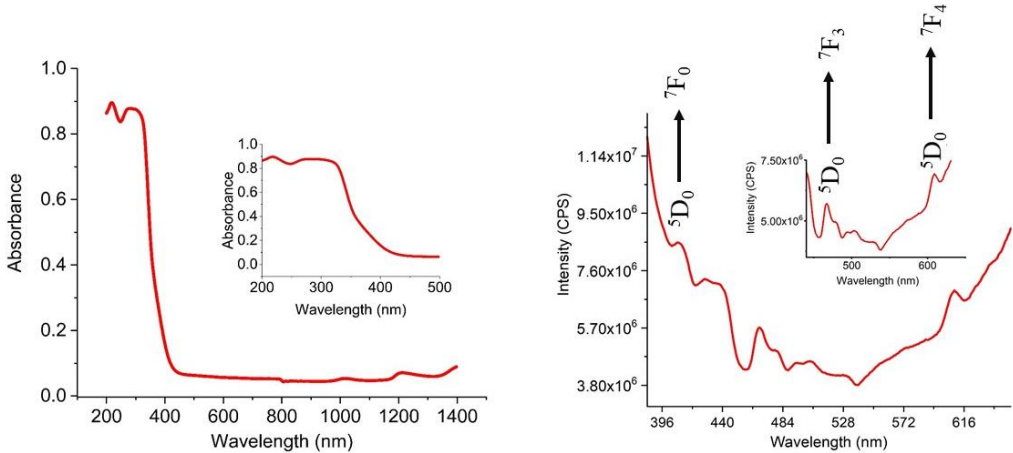


Fig. S22 Absorbance (left) and Emission(right) spectra of **2**.

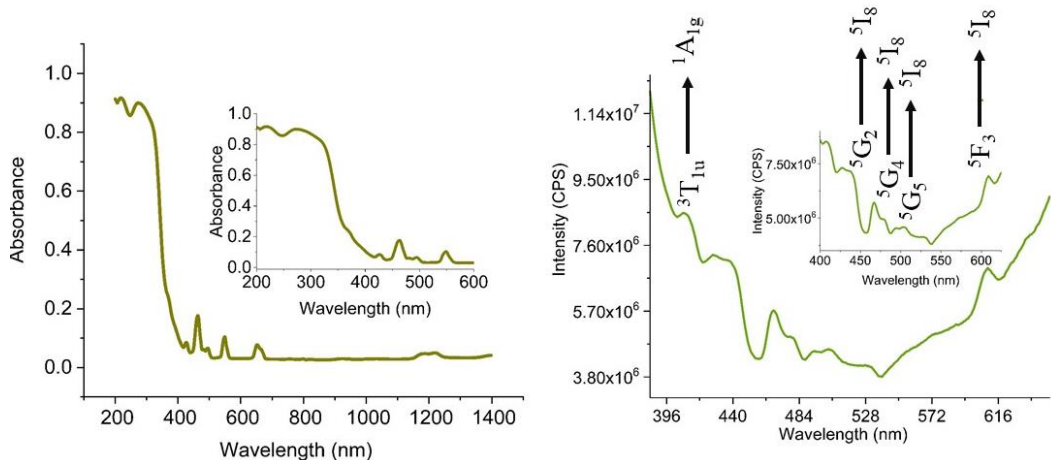


Fig. S23 Absorbance (left) and Emission(right) spectra of **3**.

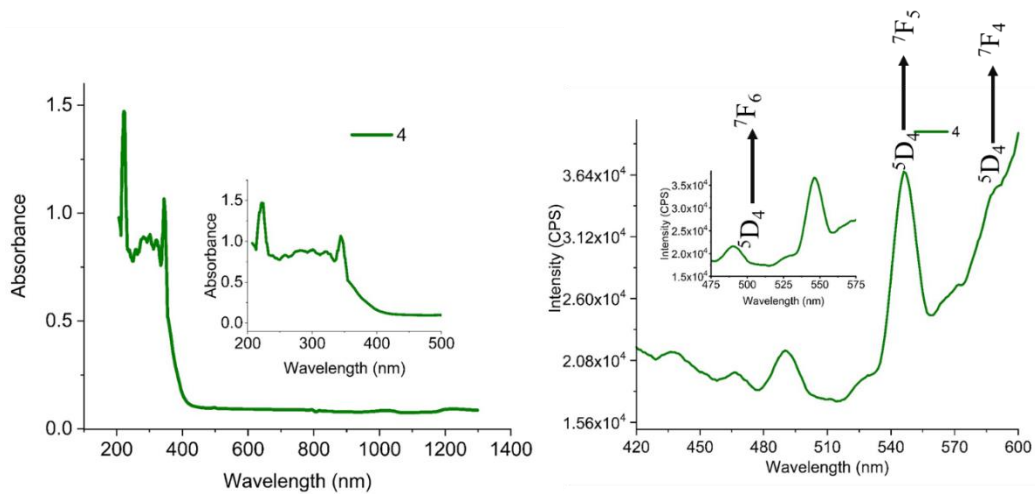


Fig. S24 Absorbance (left) and Emission(right) spectra of **4**.

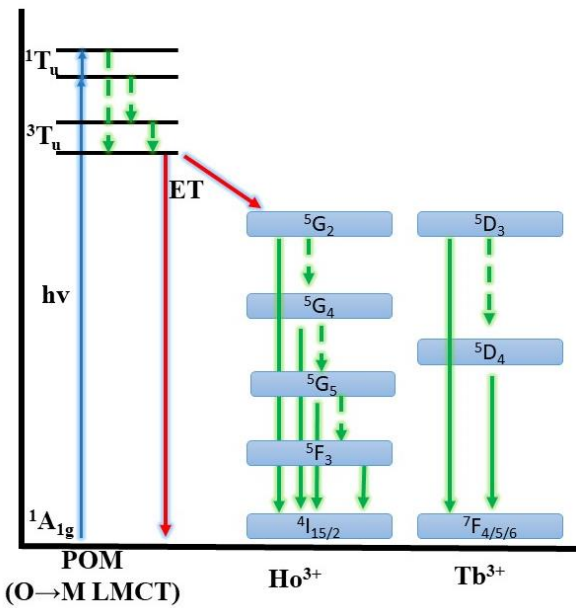


Fig. S25 Schematic representation of Energy of Different Transitions of States in **3** and **4**.

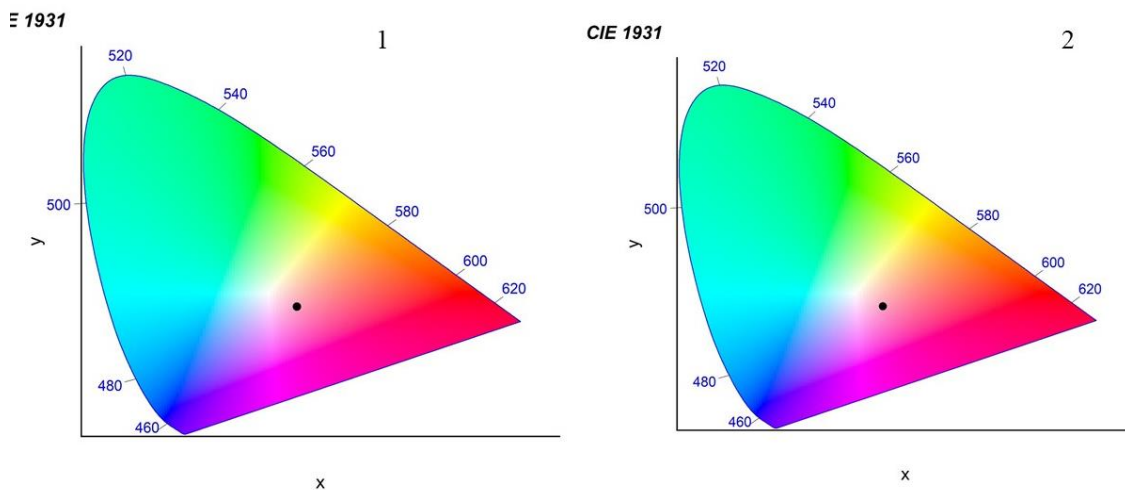


Fig. S26 The CIE 1931 chromaticity coordinates corresponding to the PL emission spectra of **1** and **2**.

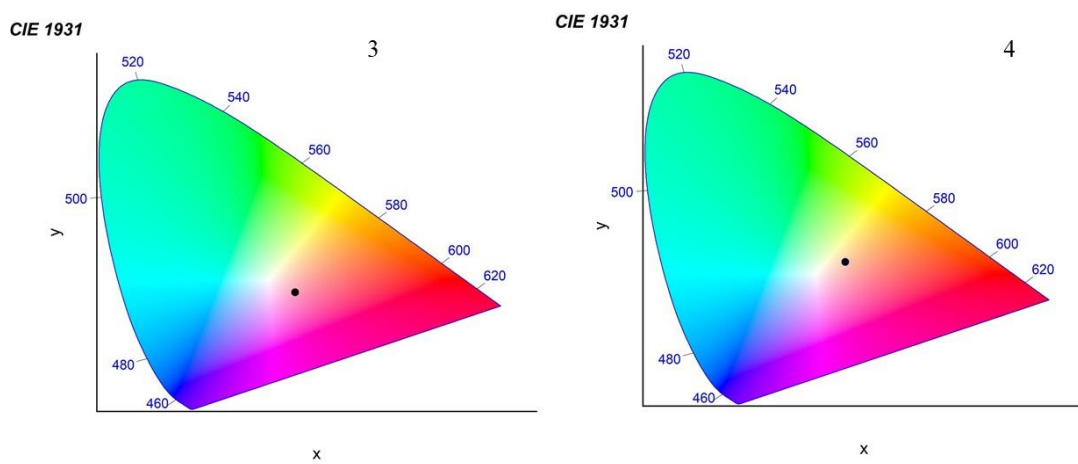


Fig. S27 The CIE 1931 chromaticity coordinates corresponding to the PL emission spectra of **3** and **4**.

Table S10: Calculated Energy of Different Transitions of States in **3**.

Transitions of states	Wavelength (nm)	Energy gap (x10 ³ cm ⁻¹)
³ T _{1u} → ¹ A _{1g}	408	30.38
⁵ G ₂ → ⁵ I ₈	435	28.50
⁵ G ₄ → ⁵ I ₈	468	26.49
⁵ G ₅ → ⁵ I ₈	505	24.55
⁵ F ₃ → ⁵ I ₈	608	20.39

Table S11: Calculated Energy of Different Transitions of States in **4**

³ T _{1u} → ¹ A _{1g}	409	30.31
⁵ D ₄ → ⁷ F ₆	492	25.20
⁵ D ₄ → ⁷ F ₅	546	22.70
⁵ D ₄ → ⁷ F ₄	584	17.12